Frustrated Orders in the Perovskite $(Bi_{0.5}Sr_{0.5})CrO_3$

Luis Ortega-San-Martin,[†] Anthony J. Williams,[‡] Alistair Storer, and J. Paul Attfield*

Centre for Science at Extreme Conditions (CSEC) and School of Chemistry, University of Edinburgh, King's Buildings, Mayfield Road, EH9 3JZ Edinburgh, U.K.

Received January 16, 2009. Revised Manuscript Received April 3, 2009

A new perovskite, $(Bi_{0.5}Sr_{0.5})CrO_3$, has been prepared at 1000 °C and ambient pressure, although $BiCrO_3$ and $SrCrO_3$ are both high pressure phases. The crystal structure is rhombohedral ($R\bar{3}c$, $a = 5.4652(5)$ and $c = 13.3502(2)$ Å at 300 K). Well-defined local Bi^{3+} displacements are evident despite an absence of long-range Bi/Sr cation order, but the degree of ferroelectric order is unclear. Long range G-type antiferromagnetic order occurs below 30 K; however, the low value of the ordered magnetic moment (1.2 μ_B), a high frustration index, and low temperature divergence of zero field and field cooled susceptibilities show that a substantial glassy component is also present.

Introduction

Chromium oxide perovskites have been the subject of substantial scientific interest, from both fundamental and practical perspectives. Like many transition metal oxides they display a range of electronic and magnetic phenomena that emerge from the coupling of spin, charge, and orbital degrees of freedom. Practical applications of chromites arise from the good p-type electrical conductivity observed at high temperature in $La_{1-x}A_xCrO_3$ (A = alkaline earth cation) phases, either in oxidizing or in reducing atmospheres. The introduction of A^{2+} cations in these phases is compensated by the oxidation of Cr^{3+} (d^3) to Cr^{4+} (d^2), and the Cr^{4+} holes are mobile via a small polaron hopping mechanism.[1,2] The robustness of this conductivity, even at high temperatures and under different atmospheres, and the thermal stability of the phases to over 2000 °C, has allowed these materials to be widely used as interconnects in solid oxide fuel cells (SOFC).[3,4] The high electrical conductivity of $La_{1-x}A_xCrO_3$ (A = Sr or Ba) has also focused attention on their possible uses as SOFC cathodes and anodes.[5,6] In addition, the high thermal stability of $LaCrO_3$ makes this material useful for high temperature heating applications.[7]

Several chromium oxide perovskites form under high pressure and temperature conditions, and recent investigations have revealed complex structural and magnetic phase diagrams. $SrCrO_3$, synthesized at pressures > 4 GPa, was initially reported as a simple cubic oxide with no magnetic order at low temperature.[8,9] However, it has recently been demonstrated to be more complex, exhibiting an orbital ordering transition with electronic phase coexistence at low temperatures.[10,11] $SrCrO_3$ is cubic and triply orbitally degenerate at high temperature but transforms to a tetragonal doubly orbitally degenerate phase which is antiferromagnetic below 35−40 K, whereas the cubic phase remains paramagnetic at low temperatures. The orbital ordering temperature (35−70 K) and the coexistence of the two electronic phases are very sensitive to lattice strain. Orbital ordering has also been observed in the more distorted $CaCrO_3$ perovskite that shows unconventional antiferromagnetic interactions below 100 K.[8,12,13]

$BiCrO_3$ also requires high pressure (4−6 GPa) conditions for bulk synthesis[14] and presents a rich phase diagram of particular interest for multiferroic properties. A structural transition from a distorted *Pnma* orthorhombic structure to a *C*2/*c* monoclinic phase is accompanied by a dielectric anomaly[15] that has been assigned to an antiferroelectric order.[16] $BiCrO_3$ also shows at least three magnetic anomalies at low temperatures, including a two step antiferromagnetic transition that is sensitive to the oxygen stoichiometry.[17] A G-type antiferromagnetic structure, in which each Cr moment is antiparallel to its six nearest neighbors, is observed below

* Corresponding author. E-mail: j.p.attfield@ed.ac.uk.
[†] Present Address: Instituto de Ciencia de Materiales de Aragón, CSIC-Universidad de Zaragoza, C/Maria de Luna 3, 50018-Zaragoza, Spain.
[‡] Present Address: Department of Chemistry, Princeton University, Washington Road, Princeton NJ 08542.

(1) Meadowcroft, D. B. *J. Phys. D.: Appl. Phys.* **1969**, *2*, 1225.
(2) Karim, D. P.; Alred, A. T. *Phys. Rev. B* **1979**, *20*, 2255.
(3) Zhu, W. Z.; Deevi, S. C. *Mater. Sci. Eng., A* **2003**, *348*, 227.
(4) Singh, P.; Minh, N. Q. *Int. J. Appl. Ceram. Technol.* **2004**, *1*, 5.
(5) Tao, S. W.; Irvine, J. T. S. *Nat. Mater.* **2003**, *2*, 320.
(6) Jiang, S. P.; Liu, L.; Ong, K. P.; Wu, P.; Li, J.; Puc., J. *J. Power Sourc.* **2008**, *176*, 82.
(7) Hayashi, S.; Sofue, S.; Yoshikado, S. *Electr. Eng. Jpn* **2002**, *139*, 18.
(8) Zhou, J.-S.; Jin, C.-Q.; Long, Y.-W.; Yang, L.-X.; Goodenough, J. B. *Phys. Rev. Lett.* **2006**, *96*, 046408.
(9) Chamberland, B. L. *Solid State Commun.* **1967**, *5*, 663.
(10) Williams, A. J.; Gillies, A.; Attfield, J. P.; Heymann, G.; Huppertz, H.; Martínez-Lope, M. J.; Alonso, J. A. *Phys. Rev. B* **2006**, *73*, 104409.
(11) Ortega-San-Martin, L.; Williams, A. J.; Rodgers, J.; Attfield, J. P.; Heymann, G.; Huppertz, H. *Phys. Rev. Lett.* **2007**, *99*, 255701.
(12) Streltsov, S. V.; Korotin, M. A.; Anisimov, V. I.; Khomskii, D. I. *Phys. Rev. B* **2008**, *78*, 054425.
(13) Komarek, A. C.; Streltsov, S. V.; Isobe, M.; Moeller, T.; Hoelzel, M.; Senyshyn, A.; Trots, D.; Fernandez-Diaz, M. T.; Hansen, T.; Gotou, H.; Yagi, T.; Ueda, Y.; Anisimov, V. I.; Grueninger, M.; Khomskii, D. I.; Braden, M. *Phys. Rev. Lett.* **2008**, *101*, 167204.
(14) Sugarawa, F.; Iida, S. *J. Phys. Soc. Jpn.* **1968**, *25*, 1553.
(15) Niitaka, S.; Azuma, M.; Takano, M.; Nishibori, E.; Takata, M.; Sakata, M. *Solid State Ionics* **2004**, *172*, 557.
(16) Kim, D. H.; Lee, H. N.; Varela, M.; Christen, H. M. *Appl. Phys. Lett.* **2006**, *89*, 162904.
(17) Belik, A. A.; Tsujii, N.; Suzuki, H.; Takayama-Muromachi, E. *Inorg. Chem.* **2007**, *46*, 8746.

10.1021/cm900148a CCC: $40.75
Published on Web 05/04/2009

Table 1. Comparison between the Rietveld Fit Results from the Centrosymmetric ($R\bar{3}c$) and Acentric ($R3c$) Structural Models[b] Used To Fit the 300 K XRD and NPD Data for $(Bi_{0.5}Sr_{0.5})CrO_3$[a]

	$R\bar{3}c$: 300 K		$R3c$: 300 K			
parameter	XRD	NPD	XRD	NPD	$R\bar{3}c$: 90 K	$R\bar{3}c$: 10 K[c]
a (Å)	5.46431(5)		5.46452(5)		5.4615(3)	5.4616(2)
c (Å)	13.3475(2)		13.3480(2)		13.3382(11)	13.3374(8)
vol (Å^3)	345.15(1)		345.18(1)		344.55(2)	344.54(1)
Bi z	0.266(1)		0.230(1)		0.25	0.25
Sr z	0.257(4)		0.259(1)		0.25	0.25
Bi/Sr U_{iso} (Å^2)	0.0206(4)		0.0225(1)		0.0274(9)	0.0275(7)
Cr U_{iso} (Å^2)	0.0004(3)		0.0008(4)		0.0008(4)	0.0008(4)
O x	0.4656(3)		0.4751(7)		0.4672(4)	0.4667(3)
O y	0		0.015(1)		0	0
O z	0.25		0.244(1)		0.25	0.25
O U_{iso} (Å^2)	0.0107(5)		0.0085(6)		0.0125(5)	0.0132(4)
R_{wp} (%)	4.0	5.1	4.0	5.1	6.3	5.0

[a] Low temperature NPD structural results (in $R\bar{3}c$) are also included. [b] Cation coordinates: Bi/Sr (0, 0, z) and Cr (0, 0, 0) in both models. [c] Cr magnetic moment $\mu_z = 1.23(8)\ \mu_B$.

109 K.[18] $La_{1-x}Bi_xCrO_3$ ($x \leq 0.35$) phases, in which the presence of Bi^{3+} induces ferroelectricity below 77 K coexisting with antiferromagnetic order, have recently been prepared at ambient pressures.[19]

We have explored the $Bi_{1-x}Sr_xCrO_3$ system with the aim of finding stable perovskite phases that may display some of the interesting properties of the high pressure end members. We report here the structural, magnetic, and transport properties of the new phase $Bi_{0.5}Sr_{0.5}CrO_3$, which is prepared under ambient pressure conditions.

Experimental Section

$(Bi_{1-x}Sr_x)CrO_3$ compositions with $0.2 \leq x \leq 0.8$ were investigated at ambient pressure using standard ceramic techniques. High purity $SrCO_3$, Bi_2O_3, and Cr_2O_3 were intimately mixed in stoichiometric quantities, pelletized, and fired under flowing nitrogen at 950 and 1000 °C for 36 h each. X-ray powder diffraction showed the formation of a single perovskite type phase only in the case of $x = 0.5$. This perovskite and secondary phases ($Sr_3(CrO_4)_2$ and binary Bi oxides) were found for $x = 0.4$ and 0.6 starting compositions, and no perovskite was evident for the $x < 0.4$ or $x > 0.6$ compositions even when synthetic conditions (firing times, temperatures, use of a more reducing 5% H_2 in Ar atmosphere) were varied. Oxygen-containing atmospheres led to the formation of non-perovskite, high valent Cr^V or Cr^{VI} oxides for all x.

Room temperature X-ray powder diffraction data on the $x = 0.5$ phase were collected in the range $15 \leq 2\theta \leq 120°$ with a step size of 0.007° and an integration time of 1.2 s per step, using a Bruker-AXS D8-series-2 X-ray diffractometer with Ge-monochromated Cu $K\alpha_1$ radiation. Neutron powder diffraction data were collected using the Super-D2B diffractometer at the Institut Laue Langevin (ILL, Grenoble, France). Neutrons of wavelength 1.5943 Å were incident on an 8 mm vanadium can contained in a helium cryostat. Patterns were collected at 10, 90, and 300 K on warming for the angular range $5 < 2\theta < 160°$ in steps of 0.05° with an overall collection time of 3.5 h. The crystal structure was analyzed by the Rietveld method[20] using the GSAS software package.[21]

Magnetic susceptibility measurements were performed using a Quantum Design MPMS-2 SQUID magnetometer while heating from 5 to 300 K in an applied field of 10 kOe. Measurements were carried out after zero field (ZFC) and field (FC) coolings. A magnetization loop was measured at 5 K.

A small sintered pellet of the sample was used for electrical resistivity measurements in a Quantum Design PPMS system. Data were collected using a current of 5 mA in $H = 0$ and 10 kOe fields using a standard 4-probe technique, from 350 down to 40 K below which the sample resistance was too large to be measured. Magnetoresistance in fields up to 80 kOe was measured at 150 and 300 K.

Results

Crystal Structure. The room temperature neutron powder diffraction (NPD) profile of $(Bi_{0.5}Sr_{0.5})CrO_3$ contains several reflections that are not observed in the X-ray diffraction (XRD) pattern and are indexed by a rhombohedral $\sqrt{2}a_p \times \sqrt{2}a_p \times 2\sqrt{3}a_p$ superstructure of the ideal cubic perovskite arrangement (cell parameter a_p). No superstructure reflections that would arise from A site ordering were observed showing that the Bi/Sr cations are not long-range ordered. A simultaneous Rietveld analysis of the XRD and NPD data was used to refine the 300 K structure of $(Bi_{0.5}Sr_{0.5})CrO_3$. The peak profiles were fitted using a modified pseudo-Voigt function, and the background was fitted with a linear interpolation function. Initial refinements using anisotropic thermal parameters showed that the Bi/Sr scattering density was elongated parallel to z, and so the Bi and Sr atoms were subsequently refined with independent z-coordinates. Both centric $R\bar{3}c$ and acentric $R3c$ models were refined-in the former case the Bi and Sr sites were split around the $z = 1/4$ mirror plane. The two models gave stable refinements with virtually identical R-factors, and results for both are shown in Tables 1 and 2. The oxygen fraction was also allowed to vary in the final stages, but it did not depart from unity within an error of 1−2% indicating that the sample is oxygen-stoichiometric.

No further distortion of the unit cell was observed upon cooling, so an $R\bar{3}c$ structural model was used to fit the 90 and 10 K NPD data. Bi and Sr z-coordinates could not be refined independently from neutron data alone and so were fixed at $z = 0.25$. The final refined parameters and residuals

(18) Belik, A. A.; Iikubo, S.; Kodama, K.; Igawa, N.; Shamoto, S.; Takayama-Muromachi, E. *Chem. Mater.* **2008**, *20*, 3765.
(19) Guo, H.-Y.; Chen, J. I. L.; Ye, Z. G.; Arrot., A. S. *J. Mater. Res.* **2007**, *22*, 2081.
(20) Rietveld, H. M. *J. Appl. Crystallogr.* **1969**, *2*, 65.
(21) Larson, A. C.; Von Dreele, R. B. *GSAS: General Structure Analysis System*, LAUR 86-748; Los Alamos National Laboratory: Los Alamos, NM, 1994.

Table 2. Selected Bond Distances (Å) and Angles (deg) for $(Bi_{0.5}Sr_{0.5})CrO_3$ at Different Temperatures in the Space Groups $R\bar{3}c$ (RT, 90 and 10 K) and $R3c$ (RT)[a]

	$R\bar{3}c$: 300 K		$R3c$: 300 K		$R\bar{3}c$: 90 K	$R\bar{3}c$: 10 K
parameter	Sr	Bi	Sr	Bi	Bi/Sr	Bi/Sr
M−O[b] × 3	2.82(4)	2.91(1)	2.63(1)	2.936(9)	2.731(2)	2.731(2)
M−O[c] × 3	2.546(3)	2.553(2)	2.562(2)	2.563(2)	2.552(2)	2.549(2)
M−O[c] × 3	2.922(2)	2.928(2)	2.917(2)	2.918(2)	2.910(2)	2.910(2)
M−O[d] × 3	2.65(4)	2.56(1)	2.85(1)	2.531(9)	2.731(2)	2.731(2)
⟨M−O⟩	2.73(2)	2.74(2)	2.74(2)	2.74(2)	2.731(2)	2.730(2)
σ(M−O)	0.15	0.16	0.15	0.19	0.13	0.13
Cr−O	1.9393(2) × 6		1.955(9) × 3 1.928(9) × 3		1.940(2) × 6	1.940(2) × 6
O−Cr−O	90.38(5)		90.1(1)−94.6(4)		90.36(1)	90.37(1)
Cr−O−Cr	168.9(1)		167.8(1)		169.4(1)	169.2(1)

[a] The root mean square deviations, σ, in the distribution of M = Bi, Sr distances to oxygen are also shown. [b−d] Oxygen atoms are at (b) $z \approx 1/12$; (c) $z \approx 1/4$; and (d) $z \approx 5/12$.

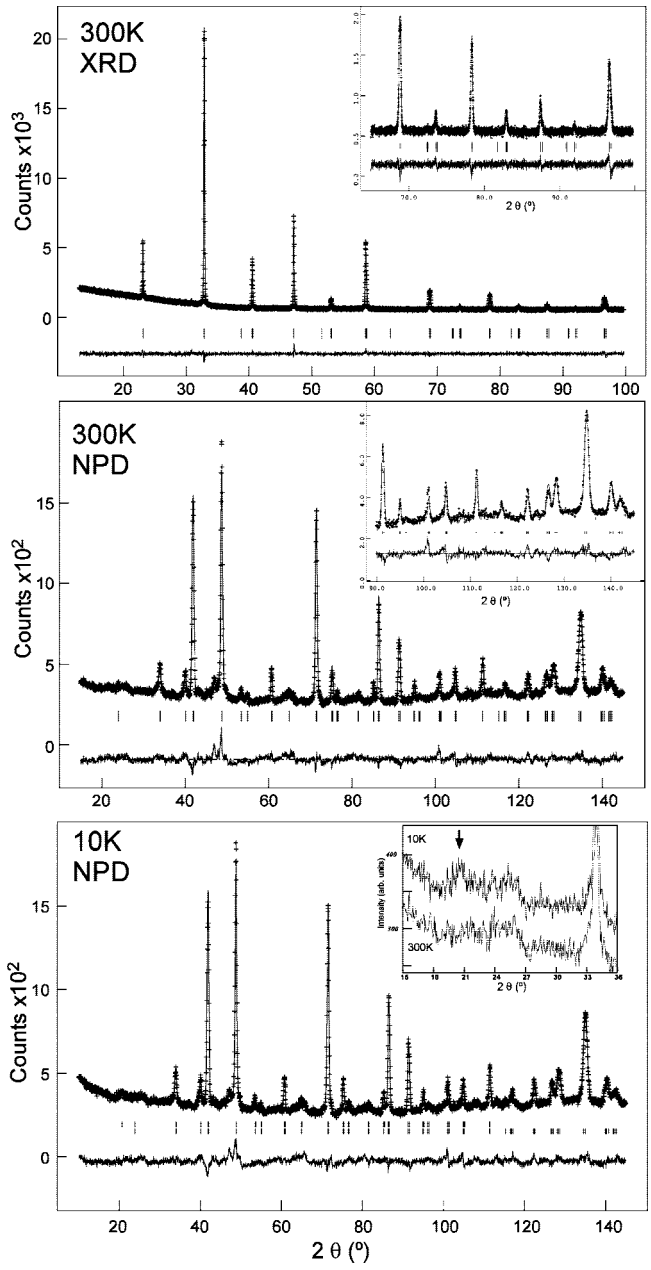

Figure 1. Rietveld fits to the X-ray (XRD) and neutron (NPD) data of $(Bi_{0.5}Sr_{0.5})CrO_3$ showing observed, calculated, and difference curves. Upper tick marks in the 10 K plot correspond to the magnetic phase, and the inset shows the ($^1/_2$ $^1/_2$ $^1/_2$) magnetic peak (arrowed). The insets to the 300 K fits show the high angle data.

Table 3. Mean Cr−O Distances at Room Temperature for Reported A CrO_3 Cr^{3+} or Cr^{4+} Perovskites, Showing the Ranges of Distances for Each State

material	mean Cr−O distance (Å)	space group	reference
$SrCrO_3$	1.912	$Fm\bar{3}m$	11, 24
$(Ca_{0.5}Sr_{0.5})CrO_3$	1.903	*P4/mmm*	24
$CaCrO_3$	1.908	*Pnma*	24
$LaCrO_3$	1.973	*Pnma*	25
$NdCrO_3$	1.973	*Pnma*	26
$GdCrO_3$	1.974	*Pnma*	27
$ErCrO_3$	1.976	*Pnma*	28
$BiCrO_3$	1.990	*C2/c*	29

are given in Table 1, and selected bond distances and angles are shown in Table 2. The observed, calculated, and difference profiles are shown in Figure 1.

The crystal structure of $(Bi_{0.5}Sr_{0.5})CrO_3$ is characterized by a tilting of the CrO_6 octahedra along the three axes of the primitive perovskite cell (described as $a^-a^-a^-$, according to Glazer's notation[22]) that results in a reduction of the Cr−O−Cr angles from the ideal value of 180° to 169°, as shown in Table 2. The Cr−O distances fall between the limits expected for tetravalent and trivalent chromium cations in the octahedral perovskite environment, $\langle Cr^{4+}-O\rangle = 1.91$ Å; $\langle Cr^{3+}-O\rangle = 1.97$ Å, respectively, as shown for the examples in Table 3. Bond valence calculations[23] yield a charge of 3.49 for the Cr site, in excellent agreement with the expected valence and further confirming the oxygen stoichiometry. No significant changes to the structure between 10 and 300 K are evident from the bond distances and angles shown in Table 2.

Magnetic Properties. The temperature dependences of the molar magnetic susceptibility χ_m and the inverse susceptibility for $(Bi_{0.5}Sr_{0.5})CrO_3$ are shown in Figure 2. χ_m follows a Curie−Weiss law, $\chi_m = C_m/(T - \theta)$, at high temperatures, and a fit to the data above 125 K yields a Curie constant of $C_m = 1.49$ cm^3·K/mol and a Weiss temperature $\theta = -480$

(22) Glazer, A. M. *Acta Crystallogr., Sect. A* **1975**, *31*, 756; *Acta Crystallogr., Sect. B* **1972**, *28*, 3384.
(23) Brese, N. E.; O'Keeffe, M. *Acta Crystallogr., Sect. B* **1991**, *47*, 192.
(24) Castillo-Martínez, E.; Durán, A.; Alario-Franco, M. A. *J. Solid State Chem.* **2008**, *181*, 895.
(25) Sakai, N.; Fjellvâg, H.; Hauback, B. C. *J. Solid State Chem.* **1996**, *121*, 202.
(26) Lufaso, M. W.; Mugavero, S. J.; Gemmill, W. R.; Yong-Jae, L.; Vogt, T.; zur Loye, H. C. *J. Alloys Compd.* **2007**, *433*, 91.
(27) Zaitseva, Z. A.; Litvin, A. L. *Dopov. Akad. Nauk B* **1978**, *11*, 994.
(28) Bertaut, E. F.; Mareschal, J. *Solid State Commun.* **1967**, *5*, 93.
(29) From Time of flight neutron diffraction data. Belik, A. A. Personal communication. May 2008.

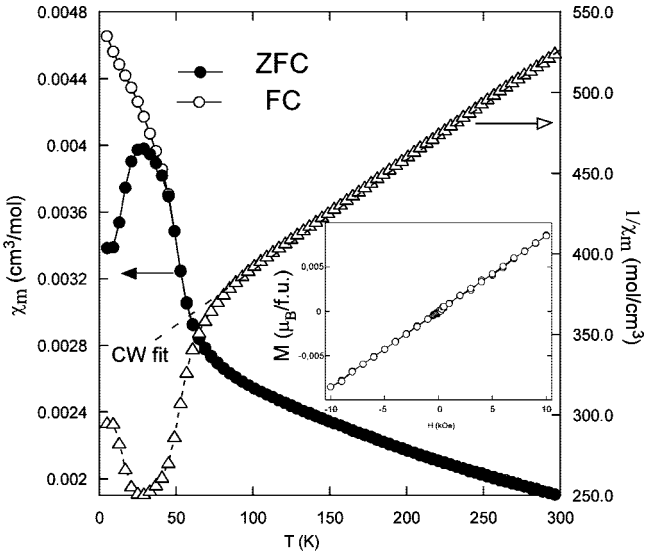

Figure 2. Temperature dependence of the of the molar magnetic susceptibility χ_m and the inverse susceptibility for $(Bi_{0.5}Sr_{0.5})CrO_3$ measured at 10 kOe. Dashed line indicates the fit to the Curie−Weiss law. Magnetization vs applied field at 5 K is shown in the inset.

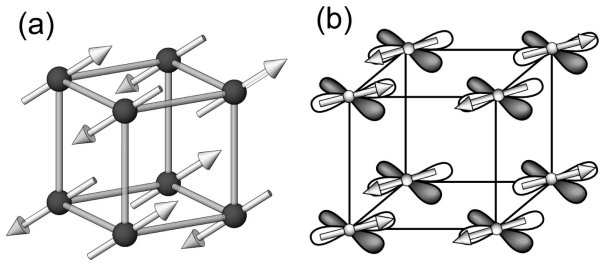

Figure 3. Chromium spin arrangements in the magnetic structures of (a) G-type $(Bi_{0.5}Sr_{0.5})CrO_3$ and (b) C-type $SrCrO_3$ also showing the t_{2g} orbital order.

K. The derived high temperature paramagnetic moment is 3.45 μ_B per $(Bi_{0.5}Sr_{0.5})CrO_3$ formula unit, consistent with the theoretical spin-only value of 3.39 μ_B for a 50:50 mixture of Cr^{4+} (2.82 μ_B) and Cr^{3+} (3.87 μ_B).

The large negative θ value indicates that strong antiferromagnetic exchange interactions are present; however, the deviation of the susceptibility on cooling below 125 K, above the Curie−Weiss limit, suggests that short-range ferromagnetic order might also occur. The ZFC and FC susceptibilities diverge below 45 K revealing a substantial glassy character to the spin order. A sharp maximum in the ZFC susceptibility and change in slope for the FC data at 30 K signifies the antiferromagnetic transition confirmed by neutron diffraction below. No hysteresis is seen in the 5 K magnetization-field loop (Figure 2, inset) confirming that the ZFC−FC divergence results from glassy rather than ferromagnetic order.

Long range magnetic order in $(Bi_{0.5}Sr_{0.5})CrO_3$ is evidenced by the observation of a weak magnetic peak in the 10 K neutron data that indexes as ($^1/_2$ $^1/_2$ $^1/_2$) on the cubic perovskite subcell. The ($^1/_2$ $^1/_2$ $^1/_2$) magnetic propagation vector corresponds to the antiferromagnetic G-type order in which each Cr spin is antiparallel to its six nearest neighbors (Figure 3) as is common in perovskites. This model fits the data well with a refined Cr moment of 1.23(8) μ_B parallel to the *c*-axis of the hexagonal setting for the supercell, although we cannot rule out other moment directions. The ordered moment is

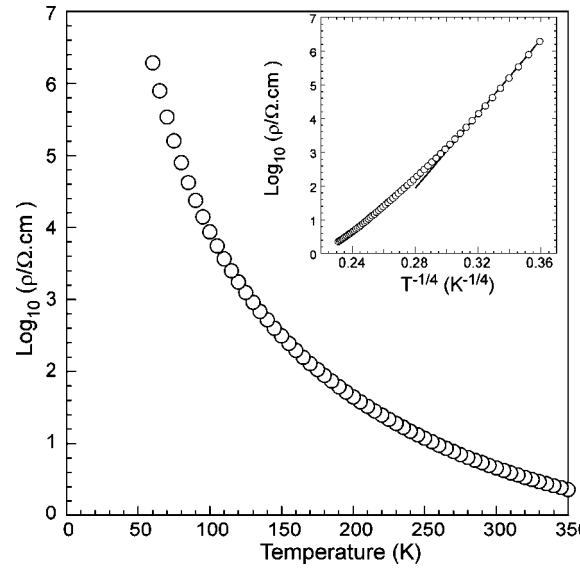

Figure 4. Temperature dependence of the electrical resistivity for $(Bi_{0.5}Sr_{0.5})CrO_3$. Inset shows the linear low temperature limit of the resistivity as expected for a three-dimensional VRH model (see text).

substantially less than the ideal value of 2.5 μ_B for an average $Cr^{3.5+}$ state, in keeping with the glassy behavior observed in the susceptibility measurements.

Transport Properties. The temperature dependence of the electrical resistivity is shown in Figure 4. Semiconducting behavior is observed and can be described at low temperatures using the Mott variable-range hopping (VRH) model:[30]

$$\rho = \rho_0\sqrt{T/T_0}\,\exp(T_0/T)^{1/(d+1)} \quad (1)$$

where d is the dimensionality of the hopping process and T_0 is the characteristic temperature (fitting parameter). The prefactor is temperature dependent but is typically neglected in comparison to the stronger temperature dependence of the exponential term. The linear variation of log ρ with $T^{-1/4}$ at low temperatures (Figure 3b) indicates that a three-dimensional ($d = 3$) process accounts well for the semiconducting behavior in this region. At higher temperature the curve deviates from linearity indicating a change in mechanism, probably to a band type semiconductor. A negligible magnetoresistance effect, <1% under a field of 80 kOe, was found at 150 and 300 K.

Discussion

This study demonstrates that the mixed A-cation $(Bi_{1-x}Sr_x)CrO_3$ perovskite may be obtained for $x = 0.5$ at ambient pressure, although the end members $SrCrO_3$ and $BiCrO_3$ require synthesis pressures of at least 4 GPa. Similar stabilization of an ambient pressure intermediate between two high pressure perovskites has been reported for $Bi(Mn_{2/3}Ni_{1/3})O_3$ in the $Bi(Mn_{1-x}Ni_x)O_3$ system.[31] Pressures up to 6 GPa are needed to prepare the Mn or Ni end members[32,33] and the $x = 0.5$ double perovskite intermediate

(30) Mott, N. F.; Davis, E. A. *Electronic Processes in Non-Crystalline Materials*, 2nd ed.; Clarendon Press: Oxford, 1979.
(31) Hughes, H.; Allix, M. M. B.; Bridges, C. A.; Claridge, J. B.; Kuang, X.; Niu, H.; Taylor, S.; Song, W.; Rosseinsky, M. J. *J. Am. Chem. Soc.* **2005**, *127*, 13790.

phase which shows multiferroic properties.[34] However, $Bi(Mn_{2/3}Ni_{1/3})O_3$, showing low temperature spin glass behavior and a ferroelectric transition at 240 °C, was prepared at ambient pressure. Another possible example is the ambient pressure phase $Bi(Fe_{0.5}Rh_{0.5})O_3$,[35] but here only the Rh end member is a high pressure (~6.5 GPa) material,[36] so whether $Bi(Fe_{0.5}Rh_{0.5})O_3$ shows a particular stability is unclear.

In the case of $(Bi_{1-x}Sr_x)CrO_3$, the two end members require high pressure stabilization for different reasons. For $BiCrO_3$, and most other $BiMO_3$ perovskites, high pressure is needed to force Bi^{3+} into the high coordination, symmetric A-site perovskite environment, whereas for $SrCrO_3$ pressure is needed to force octahedral coordination for Cr^{4+}, which tends to be tetrahedral in ambient pressure oxide structures. Substitution of $Sr^{2+}$for Bi^{3+}which is very stable in perovskite A sites and of d^2 Cr^{4+} by d^3 Cr^{3+}, which is very stable in octahedral environments, leads to a mutual stabilization of the perovskite structure. The perovskite phase is only observed for a very narrow range of compositions near $x = 0.5$, but there is no evidence for order of Bi/Sr cations or of Cr^{3+}/Cr^{4+} charge states that would signify a line phase at this composition. Instead, the balance of the two substitutional factors, plus the maximization of configurational entropy stabilization at $x = 0.5$, appear to account for the formation of this phase. We note that long-range charge and orbital order can be observed despite Bi/Sr disorder in manganites, for example, $Bi_{0.75}Sr_{0.25}MnO_3$,[37] but neither long-range electronic order is evident in $(Bi_{0.5}Sr_{0.5})CrO_3$.

The rhombohedral perovskite distortion observed in $(Bi_{0.5}Sr_{0.5})CrO_3$ is intermediate between the highly distorted $BiCrO_3$ and the undistorted $SrCrO_3$ structures. The observed sequence of phase transitions from $x = 1$ to 0 in the $Bi_{1-x}Sr_xCrO_3$ system, $Pm\bar{3}m \rightarrow R\bar{3}c \rightarrow C2/c$, is consistent with the decreasing perovskite tolerance factor[38] as Sr^{2+} is replaced by smaller Bi^{3+} while Cr^{4+} is replaced by larger Cr^{3+}.[39] The $Pm\bar{3}m \rightarrow R\bar{3}c$ transition is often observed in perovskites and is continuous, but the $R\bar{3}c \rightarrow C2/c$ change is discontinuous and intermediate symmetry phases (e.g., the common orthorhombic *Pnma* superstructure) may be accessible in high pressure $0 < x < 0.5$ compositions. The $Pm\bar{3}m \rightarrow R\bar{3}c \rightarrow Pnma$ symmetry descent is observed in the related $SrCr_{1-x}Ru_xO_3$ system.[10]

The combined refinement of the rhombohedral $(Bi_{0.5}Sr_{0.5})CrO_3$ structure using X-ray and neutron data shows that the Bi^{3+} ions are significantly displaced from the normal (0, 0, $^1/_4$) A-cation position of the $R\bar{3}c$ perovskite superstructure. These may be described in two opposite limits. Splitting the Bi and Sr sites in the centric space group $R\bar{3}c$ models a paraelectric phase in which Bi^{3+} ions are randomly displaced in the $+z$ or $-z$ directions. The refined coordinates (Table 1) and the derived distances (Table 2) show that a significant "lone pair" displacement of 0.2 Å is observed for Bi^{3+}, whereas the Sr^{2+} z-coordinate is within error of the average $z = 1/4$ plane. The alternative model in acentric space group $R3c$ has all of the Bi displacements parallel, corresponding to a ferroelectric structure as found for $BiFeO_3$. The models do not allow truly independent determinations of the Bi^{3+} and Sr^{2+} coordination environments as the oxygen coordinates adopt average values which impose near-equal average Bi−O and Sr−O distances (Table 2). However, it is notable that the root-mean-square deviations in the distribution of M = Bi, Sr distances to oxygen, σ(M−O), are slightly greater for Bi, as expected for distortion of the Bi^{3+} environment by lone pair effects. The two models give equally good fits, so the degree of ferroelectric order in $(Bi_{0.5}Sr_{0.5})CrO_3$ cannot be determined experimentally from the present data. The order is likely to be intermediate between these totally disordered and ordered extremes, with Sr-substitution substantially frustrating the ferroelectric order in the hypothetical $BiCrO_3$ analogue of $R3c$ $BiFeO_3$. Further experiments will be needed to determine the degree of ferroelectric order in $(Bi_{0.5}Sr_{0.5})CrO_3$ and whether a high temperature Curie transition is present. Electron microscopy will also be valuable to establish whether local ordering of A-cations, their displacements and Cr^{3+}/Cr^{4+} charge states occurs. The presence of some diffuse scattering features in the background of the neutron profiles (Figure 1) indicates that local order may be present.

$(Bi_{0.5}Sr_{0.5})CrO_3$ is semiconducting with three-dimensional variable range hopping behavior at low temperatures consistent with small polaron mobility of Cr^{4+} holes, as found in other Cr^{3+}/Cr^{4+} oxides. The Weiss temperature $\theta = -480$ K is typical of strongly antiferromagnetic oxides such as $LaCrO_3$ ($T_N = 320$ K); however, $(Bi_{0.5}Sr_{0.5})CrO_3$ has a much lower $T_N = 30$ K. This evidence of magnetic frustration, the index $|\theta|/T_N$, has a value of 16 corresponding to strongly frustrated magnetism.[40] Despite this, neutron diffraction confirms that long-range spin order occurs, but the reduction of the ordered moment to only half of the theoretical value and the divergence of zero and field cooled susceptibilities confirm that there is a substantial glassy component to the spin order. Only antiferromagnetic Cr−O−Cr π-superexchange interactions are expected between t_{2g}^3 Cr^{3+} ions, leading to G-type order as observed in $BiCrO_3$ ($T_N = 110$ K).[41] However, the degenerate t_{2g}^2 configuration of Cr^{4+} may lead to orbital order and both ferro- and antiferromagnetic Cr−O−Cr exchange pathways; for example, $SrCrO_3$ shows partial orbital order and a C-type magnetic order ($T_N \approx 35$ K) with both types of exchange evident (Figure 3b). $(Bi_{0.5}Sr_{0.5})CrO_3$ still has sufficient, strong antiferromagnetic Cr−O−Cr π-superexchange interactions to drive long-range G-type order, but the presence of some Cr^{3+}−O−Cr^{4+} and Cr^{4+}−O−Cr^{4+} ferromagnetic interactions associated with the localized Cr^{4+} t_{2g}-holes leads to substantial frustration and local magnetic disorder.

(32) Ishiwata, S.; Azuma, M.; Takano, M.; Nishibori, E.; Takata, M.; Sakata, M.; Kato, K. *J. Mater. Chem.* **2002**, *12*, 3733.
(33) Atou, T.; Chiba, H.; Ohoyama, K.; Yamaguchi, Y.; Syono, Y. *J. Solid State Chem.* **1999**, *145*, 639.
(34) Azuma, M.; Takata, K.; Saito, T.; Ishiwata, S.; Shimakawa, Y.; Takano, M. *J. Am. Chem. Soc.* **2005**, *127*, 8889.
(35) Filoti, G.; Kuncser, V.; Rosenberg, M.; Schinzer, C.; Kemmler-Sack, S. *J. Alloys Compd.* **1997**, *256*, 86.
(36) Longo, J. M.; Raccah, P. M.; Kafalas, J. A.; Pierce, J. W. *Mater. Res. Bull.* **1972**, *7*, 137.
(37) Goff, R. J.; Attfield, J. P. *J. Solid State Chem.* **2006**, *179*, 1369.
(38) Mitchell, R. H. *Perovskites modern and ancient*; Almaz Press: Ontario, 2002.
(39) Shannon, R. D. *Acta Crystallog., Sect. A* **1976**, *32*, 751.
(40) Greedan, J. E. *J. Mater. Chem.* **2001**, *11*, 37.

In conclusion, $(Bi_{0.5}Sr_{0.5})CrO_3$ demonstrates a notable stabilization of the perovskite structure through the mutually beneficial substitutions of Sr^{2+} for Bi^{3+} and of Cr^{4+} for Cr^{3+} in the high pressure end members, but these substitutions without long-range Bi^{3+}/Sr^{2+} order result in frustration of the ferroelectric and magnetic orders. The presence of long-range antiferromagnetic order and possible ferroelectricity demonstrates that $(Bi_{0.5}Sr_{0.5})CrO_3$ might show some evidence of multiferroism, although the coupling is likely to be very weak.

Acknowledgment. This work has been funded by EPSRC and the Leverhulme Trust. The authors gratefully acknowledge Dr. Alan Hewat (ILL, Grenoble) and Mr. Wei-Tin Chen for assistance with neutron data collection.

CM900148A

(41) Baettig, P.; Ederer, C.; Spaldin, N. A. *Phys. Rev. B* **2005**, *72*, 214105.